Graphene oxide-containing chitosan@HKUST-1 beads with increased chemical stability for CO2 capture

Yassine Khadiri, Alexandre Legrand, Christophe Volkringer, A. Anouar, Sebastien Royer, A. El Kadib, Thierry Loiseau, Jérémy Dhainaut

Graphene oxide-containing chitosan@HKUST-1 beads with increased chemical stability for CO_2 capture

Y. Khadiri,[a,b] A. Legrand,[a] C. Volkringer,[a] A. Anouar,[b] S. Royer,[a] A. El Kadib,[b] T. Loiseau,[a] J. Dhainaut[a]

[a] *Univ. Lille, CNRS, Centrale Lille, Univ. Artois, UMR 8181 - UCCS - Unité de Catalyse et Chimie du Solide, F-59000 Lille, France.*
[b] *Euromed University of Fes, UEMF, Morocco.*

Keywords: Metal-Organic Framework; Graphene oxide; Shaping; CO_2 adsorption; Chemical stability

Highlights:

- ✓ In-situ growth of HKUST-1 MOF within chitosan matrix
- ✓ Improved resistance to hydrolysis by addition of graphene oxide
- ✓ High CO_2 adsorption capacity reached (2.6 $mmol.g^{-1}$ at 298 K, 1 bar)

Abstract

HKUST-1 MOF was crystallized within chitosan matrix to form xerogel beads using an *in-situ* growth approach. Under mild conditions, CS@HKUST-1 xerogel beads exhibit high specific surface areas (S_{BET}) up to 923 $m^2.g^{-1}$. By further incorporating graphene oxide (GO) to form ternary CS-GO@HKUST-1 xerogel beads, the HKUST-1 MOF structure remained stable for up to two days in a water solution at room temperature, whereas the MOF powder and CS@HKUST-1 xerogel beads underwent significant framework collapse within a day. CO_2 adsorption measurements on these xerogel beads also show promising CO_2 uptakes, surpassing 2.5 $mmol.g^{-1}$ at 298 K and 1 bar. Moreover, these composites could be regenerated for more than 10 cycles without any loss of quantity adsorbed.

Introduction

Energy production predominantly relies on fossil fuels like oil, natural gas, and coal. However, the increasing energy needs, driven by the population growth and industrialization, have led to the depletion of these resources. This has in turn heightened environmental risks through the intensive release of waste and greenhouse gases into the atmosphere, with carbon dioxide (CO_2) accounting for over 80% of greenhouse gases, making it the predominant origin of global warning [1-3]. Thus, reduction of CO_2 emissions, to contain the global warning most dramatic effects, is no more an option. To date, CO_2 capture by amine or porous materials is one of the main solutions developed as it is relatively simple to implement at large scale and it allows the recovery and reuse of CO_2 [4]. Zeolites [5], activated carbons [6], mesoporous silicas [7], and metal-organic frameworks (MOFs) [8-10] are among the most promising solid adsorbents. MOFs are formed by combining organic linkers and metallic (or metal oxide) precursors, resulting in porous crystalline networks. They typically present larger pores than zeolites, high surface areas, diverse chemical functionalities, and structural diversity [11-12]. These characteristics justify their potential applications across various fields and position them competitively compared to other porous materials [13].

Being synthesized in 1999 through the coordination of trimesic acid (H_3BTC) and copper ions [14], HKUST-1 (known also as MOF-199) stands as one of the most investigated MOFs. HKUST-1 is valued for its high specific surface area (that could reach up to 1800 $m^2.g^{-1}$), facile synthesis using different processes [15-16], and the presence of open metal sites (OMSs) that function as Lewis acid sites [17]. These characteristics collectively position HKUST-1 as a leading candidate for gas adsorption applications, particularly for CO_2 capture however in dry conditions [18-19].

For industrial applications of MOFs and facilitate their handlings, many strategies have been proposed to prepare MOF solids as membranes, monoliths, pellets, granules, foams and beads, starting from the as-made powder [20-23]. However, using as-synthesized MOFs often leads to porosity loss and structural damage due to the application of pressure and the use of binders blocking pores access. In contrast, the *in-situ* growth of MOFs over substrates such as biopolymers allows easier shaping as porous films, monoliths, and microspheres [24], giving nanocomposites in which the properties of the pristine MOF are preserved. Biopolymers such as chitosan (CS) are attractive substrates because they are biocompatible, biodegradable, largely available, and recognized for their easy gelation properties [25-26]. Moreover, the large distribution of functional groups (especially NH_2 and OH) of CS enables effective interaction with metal ions through weak bonding [24,27]. These highly-dispersed metal ions can further

be used as precursors to grow MOF crystals in the presence of the adequate organic linker [28-29].

On the other hand, MOFs chemical stability to hydrolysis, acids, bases, and other chemicals also poses significant challenges. Among them, HKUST-1 is not stable when exposed to water as it leads to the hydrolysis of the Cu-BTC bonds due to weak metal coordination bonds [30-32]. To circumvent this issue, hydrophobization of the solids surface or the addition of a second material to stabilize the MOF are currently investigated solutions [32-35]. For instance, graphene oxide (GO), a single layer of graphite oxide, has been proposed as a nucleation site for the growth of MOFs [36]. Especially, strong interfacial interaction between metal ions and the functional groups of GO (carbonyl, carboxyl, and hydroxyl) is expected to strengthen the hydrolytic stability of the resulting composite [37].

Herein, we demonstrate that CS@HKUST-1 composites prepared *via* the *in-situ* growth route under mild conditions allows producing robust self-standing xerogels (densified microspheres) with high porosity following simple atmospheric drying. Moreover, the addition of graphene oxide to form ternary CS-GO@HKUST-1 composites was undertaken and its effect over the hydrolytic stability and the mechanical beads resistance was investigated. The preservation of porosity of the binary and ternary composites were also tested by N_2 and CO_2 adsorption.

Experimental details

Synthesis methodology. Composites were synthesized following an *in-situ* crystal growth method previously reported [28], with few modifications. CS@HKUST-1 binary composite beads were synthesized as follow: firstly, an appropriate amount of $Cu(NO_3)_2 \cdot 3H_2O$ was dissolved in 15 ml of distillated water. Under magnetic stirring, 0.5 g of CS and 0.8 ml of acetic acid were then added. The mixture was kept under magnetic stirring (600 rpm) at 30 °C for one night. Black CS@CuO beads were formed by coagulation of the viscous solution following its dropwise addition into an alkaline solution of NaOH (4M, 60 ml). After magnetic stirring (50 rpm) for 1 h, the beads were washed with distillated water several times until the pH of the elution solution becomes neutral, and then dehydrated by immersing them in three different ethanol-water (E/W) mixtures for 20 min each, with increasing ethanol volume ratio (10%, 30%, 50%). The beads were then introduced into a solution of H_3BTC (n(BTC)/n(Cu) = 0.76) solubilized in 40 ml of a E/W mixture (50% v:v) for 48 h at 40 °C under a stirring of 50 rpm. The resulting HKUST-1 containing beads were washed three times with 30 ml of a E/W mixture (50% v:v) to remove the unreacted H_3BTC. Finally, they were immersed in a E/W mixture

(75% v:v) for 20 minutes before being stored in 20 ml of pure ethanol. These alcogels were finally dried at room temperature for 24 h (main synthesis steps are presented in Figure S1). The xerogels, showed in Figure 1, were referred to CS@HKUST-1[n(NH_2):n(Cu)] with the following molar ratios: [2:1], [1:1], [1:2] and [1:3]. Above this ratio, the spherical shape of the resulting solids is lost as a result of inappropriate viscosity.

Figure 1. CS@HKUST-1[n(NH_2):n(Cu)] xerogels. From left to right: CS@HKUST-1[2:1], [1:1], [1:2], and [1:3].

For comparison purpose pure chitosan (CS) and chitosan mixed with copper (II) nitrate trihydrate (CS@CuO[1:2]) beads, in addition to pristine HKUST-1, were also prepared. GO was incorporated into chitosan (CS)-based composites at the optimized [n(NH_2):n(Cu)] ratio to form ternary CS-GO@HKUST-1 composites (Figure S1). Details of syntheses and characterization conditions are given in ESI.

Chemical stability tests. Chemical stability was evaluated by immersing 300 mg of beads in 8 ml of various solvents (water, acetone, ethanol, and DMF) at room temperature (20 ± 2 °C) for different durations (1-3 days, or 2 months). Following immersion, the composite beads were retrieved and dried at room temperature before analysis.

CO_2 sorption tests. CO_2 sorption isotherms were determined under static conditions using a Micromeritics ASAP 2020 system. The samples were first activated for one night at 393 K under secondary vacuum, and the measurements were then carried out at 298 K. Additionally, the isosteric enthalpy of adsorption of the leading composites were calculated from isotherms measured at 273, 283, and 298 K. To assess the recyclability of the microspheres towards CO_2 sorption, an activation step was conducted at 373 K under secondary vacuum for one night between sorption measurements.

Result and discussion

Binary composites (CS@HKUST-1). Powder XRD patterns (Figure 2a) of the binary CS@HKUST-1 xerogels all exhibit the characteristic Bragg peaks of HKUST-1, providing strong evidence of the successful crystallization of MOF particles grown within the chitosan matrix [28]. Unlike the sharp and narrow reflections observed in the case of the pristine HKUST-1 powder, the xerogels XRD patterns present broader peaks which could indicate the

formation of smaller HKUST-1 particles confined inside the CS beads as already observed [29]. In the case of CS@HKUST-1[1:3], additional peaks at 2θ= 18.1°, 28.5°, 31.1°, 36.7° and 43.0° are observed. Most of them are attributed to the presence of unreacted Cu_2O (see Figure 2a) [38], others may correspond to the formation of a copper-trimesate complex.

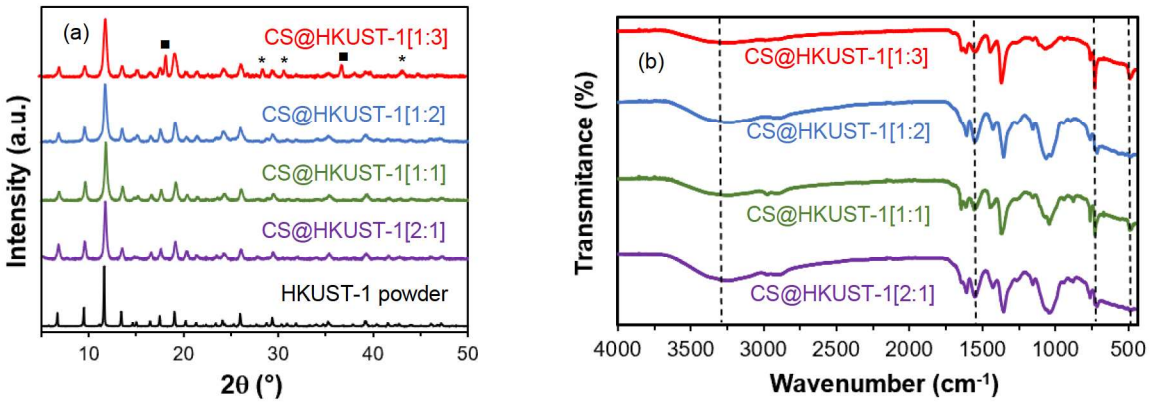

Figure 2. (a) PXRD patterns and (b) FTIR spectra of CS@HKUST-1[n(NH_2):n(Cu)] composites. * = Cu_2O, ▪ = attributed to copper-trimesate complex.

The successful crystallization of HKUST-1 within chitosan was further confirmed by FTIR spectroscopy analyses (Figure 2b and S2). One can observe the bands related to RHN-C=O (amide I at 1651 cm^{-1}) and NH_2 (amide II at 1584 cm^{-1}) functionalities characteristics of chitosan [39], and a broad band (3010-3660 cm^{-1}) assigned to N-H of CS and O-H vibrations common between CS and HKUST-1 (from physisorbed H_2O) [40]. Moreover, all composites display typical bands of HKUST-1 like Cu-O stretching vibration bond at 730 cm^{-1}, and trimesate (BTC) bands detected between 730 and 1700 cm^{-1}, with peaks around 1366 and 1646 cm^{-1} being ascribed to the stretching vibration of C=O bonds [41]. The slight shift of NH_2 vibration bands towards lower wavenumbers with the increase of MOF loading suggests a transfer of electron density from NH_2 to the metal site in HKUST-1 ($NH_2 \rightarrow Cu$) [42]. This confirms the intimate interplay between the biopolymer and both the metal and the linker of HKUST-1 during crystallization.

After drying under air, the xerogel beads volume shrank at different rates depending on the [n(NH_2):n(Cu)] ratio (Figure S3). As shown in Table S1, unlike pure CS beads displaying a dramatic shrinkage up to 62%, the CS@HKUST-1 composites retain better their initial shape and dimensions. The shrinkage value varies with the HKUST-1 loading, ranging from 44% for the lowest HKUST-1 content (ratio [2:1]) down to 23% for CS@HKUST-1[1:3]. Composite beads with copper oxide embedded in the chitosan matrix (CS@CuO[1:2]) have also been prepared similarly. As shown in Figure S4, a significant diameter shrinkage (60%) of the beads is observed after drying, similar to that observed for pure chitosan beads. Thus, the presence of

copper oxide does not prevent shrinkage, while the growth of HKUST-1 particles within CS beads improves the shape stability and enables better resistance against the capillary forces occurring on the open porous network of chitosan during air-drying.

The typical thermal behavior under air of the prepared samples is shown in Figure S5. The first weight loss observed at about 120 °C corresponds to the removal of residual solvents. The second weight loss event, observed at nearly 200 ± 15 °C, is assigned to the beginning of chitosan degradation [43], while a third weight loss stage observed starting at about 300 °C corresponds to the combustion of the trimesate linker and the formation of CuO [44]. Complete degradation of chitosan ends at about 400 °C for the composites and at 610 °C for pure chitosan beads. Based on the dehydrated HKUST-1 formula [$Cu_3(BTC)_2$], and the final residue (CuO) content, the original amounts of HKUST-1 within the composites can be estimated (Table S2), and about 63 wt.% of HKUST-1 could be loaded within the chitosan xerogels with no trace of impurity (for the CS@HKUST-1[1:2] ratio). In the case of CS@HKUST-1[1:3], the 73.4 % loading found from TGA is overestimated due to the presence of an additional Cu-based phase. SEM analyses (Figures 3 and S6) of CS@HKUST-1[1:2] show crystals of about 16 µm with a octahedral shape typical of HKUST-1. The crystals are uniformly dispersed within the beads while their outer surface is mostly particles-free. By decreasing the amount of copper ($n(NH_2)$:n(Cu) > 1:2), beads cross-sections show embedded HKUST-1 particles (Figure S6). On the other hand, increasing of the amount of copper (CS@HKUST-1[1:3]) results in the growth of HKUST-1 crystals, not only within the spheres but also at their external surface (Figure S6). Moreover, in the latter material, the size of the crystals at the surface is smaller (2.5 µm) than in the core (7 µm). This may arise from increased nucleation kinetic at the surface thus forming more but smaller crystals. EDS analysis of copper, carbon, oxygen and nitrogen reveals a uniform distribution of all these elements within the beads (Figure S7).

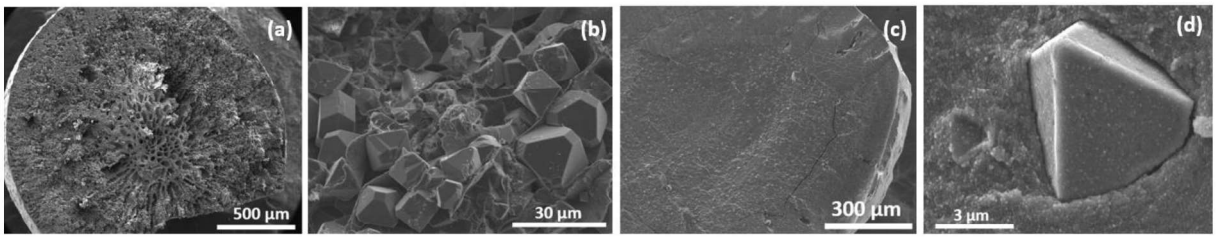

Figure 3: SEM cross-section images of (a-b) CS@HKUST-1[1:2] and (c-d) CS@HKUST-1[2:1].

Of note, it has been reported that the drying step (vacuum oven, freeze drying, supercritical CO_2) strongly affects the final porous structure of the composite, and consequently its catalytic and adsorptive performances [25,29]. Indeed, following classical drying under air, the textural

properties of the resulting xerogels are significantly lower than when CO_2 supercritical drying (aerogels) or freeze-drying (cryogels) were used, the two latter preserving an open porosity [29,45]. N_2 physisorption isotherms (Figure 4 and Table S3) reveal that only CS@HKUST-1 with $n(NH_2):n(Cu)$ ratio < 1 (MOF loadings ≥ 63 wt.%) give composites with a significant porosity at 77 K. For lower MOF loadings, the HKUST-1 particles are completely embedded by the chitosan matrix, resulting in significant pore blocking, as observed from SEM. The absence of porosity in the case of CS@CuO[1:2] and CS xerogels is also expected due to the consequent shrinkage of the beads observed after drying and the absence of microporosity.

CS@HKUST-1[1:2] and CS@HKUST-1[1:3] are mostly microporous, as characterized by type I isotherms [46], even if a second lower uptake from p/p_0 = 0.8 with CS@HKUST-1[1:2] indicates the presence of interparticular mesopores from 35 nm leading to capillary condensation (Figure S8). The specific surface areas (measured up to 849 and 1033 $m^2.g^{-1}$ for [1:2] and [1:3], respectively) are higher than those of most CS@MOF composites previously reported, whatever the drying route used (Table S4). When taking the MOF loadings into account (Table S2), these surface areas even reach 1343 $m^2.g^{-1}_{(MOF)}$ for CS@HKUST-1[1:2]. For comparison, the specific surface area of pristine HKUST-1 prepared in the same conditions (low temperature and atmospheric pressure) reached 1555 $m^2.g^{-1}$, similar to classical HKUST-1 obtained under solvothermal conditions [47]. Moreover, the pore sizes distribution of these composites (Figure S8) were practically the same as those of HKUST-1, with a monomodal distribution at around 12.0-12.4 Å (pores < 10 Å not probed by our apparatus). Thus, accessibility to the microporous network of HKUST-1 is only slightly reduced by the presence of the CS matrix.

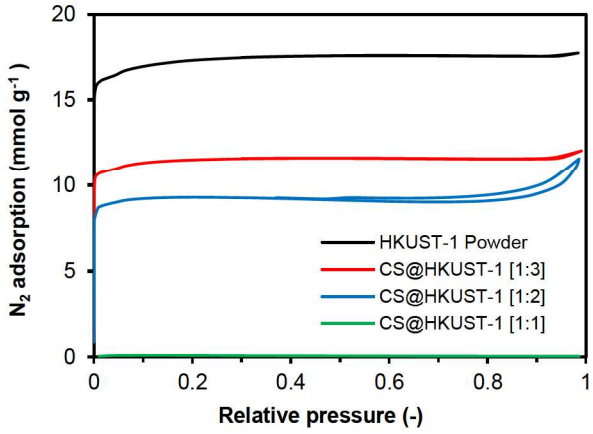

Figure 4. N_2 physisorption isotherms of HKUST-1 and the CS@HKUST-1 xerogels with different CS@HKUST-1 ratio, measured at 77 K.

Besides the drying method, other key parameters can affect the porosity of the composite beads, and are related to the type of chitosan (low-to-high molecular weight, deacetylation degree) and its concentration, the concentrations of NaOH and acetic acid, the time of conservation of the beads in the alkaline solution, solvent exchange, and the molar ratio BTC/Cu [48-49]. In addition, the synthesis temperature may also play a crucial role. For instance, in the case of HKUST-1 powder, a lower synthesis temperature was found to prevent the formation of impurities such as Cu_2O [16,50].

To test this hypothesis, CS@HKUST-1[1:2] was prepared at room temperature (CS@HKUST-1(25)) and at 80 °C (CS@HKUST-1(80)) after addition of the organic linker solution to CS@Cu beads (synthesis details are given in ESI). Indeed, when the synthesis temperature was increased to 80 °C, the XRD diffractograms (Figure S9) revealed several additional Bragg reflections observed at 2θ = 10.2°, 27.3° and 37.7°, whereas a pure phase of HKUST-1 is observed at lower temperatures. Nitrogen sorption isotherms (in Figure S10) also underline significant differences between the composite prepared under mild conditions (S_{BET} = 849 and 923 $m^2.g^{-1}$ at 40 °C and 25 °C, respectively) and the reflux-prepared composite (80 °C - S_{BET} = 524 $m^2.g^{-1}$). Thus, a mild synthesis temperature is recommended to prepare such CS@HKUST-1 composites.

Ternary composites (CS-GO@HKUST-1). Following this, composites containing graphene oxide (GO) were considered. GO was successfully prepared following the Hummers method, as demonstrated by PXRD, FTIR and Raman spectroscopy (Figure S11), and then incorporated into the CS@HKUST-1 composite synthesized at the optimal temperature and CS:Cu ratio (see ESI).

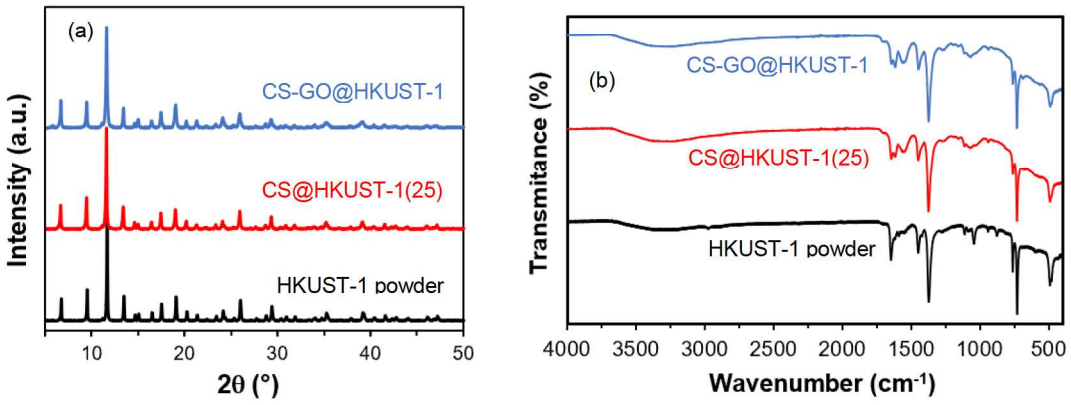

Figure 5. (a) PXRD patterns and (b) FTIR spectra of pristine HKUST-1, CS@HKUST-1(25) and CS-GO@HKUST-1 xerogels.

The efficient synthesis of composites containing the HKUST-1 crystalline phase was evidenced by the characteristic Bragg peaks of HKUST-1 observed by PXRD (Figure 5a). As in the case of CS@HKUST-1(25), SEM images of the CS-GO@HKUST-1 ternary composites reveal well-dispersed HKUST-1 octahedral particles within the beads (Figure S12). Furthermore, SEM analysis confirms the presence of graphene oxide sheets within the ternary xerogels (see flakes surrounded with red circles - Figure S12). FTIR spectrum aligns with PXRD results and is comparable to the FTIR spectra of CS@HKUST-1 xerogels (Figure 5b). Raman spectroscopy (Figure S13a-b) shows the emergence of not only the characteristic bands of HKUST-1 through Cu-Cu vibration bonds at 495 cm^{-1}, two bands at 1000 and 1615 cm^{-1} assigned to benzene cycle C=C bonds, stretching vibrations of C-H at 820 cm^{-1} and of –COO at 1460 and 1544 cm^{-1} [51], but also the presence of D (1353 cm^{-1}) and G (1594 cm^{-1}) bands characteristic of GO and indicating its successful incorporation within CS-GO@HKUST-1 composite. Furthermore, the observed flakes have a similar Raman signature as GO sheets (Figure S13b). N_2 physisorption isotherms (Figure S14) demonstrate a slight decrease in specific surface area and pore volume following the addition of GO (878 instead of 923 $m^2.g^{-1}$), in line with its content in the xerogel beads.

Chemical and mechanical stability of binary and ternary systems. The HKUST-1 MOF is known for its low resistance toward hydrolysis, especially under high relative humidity (RH ≥ 80 %) and low temperature (≤ 100 °C), where its structure is rapidly hydrolyzed into a dense hydrated copper trimesate phase following the breakage of the metal-ligand bonding by water molecules [52-54]. Notably, temperatures above 100 °C significantly inhibit the hydrolysis process [54]. In the presence of liquid water (20 mol.% relative to the amount of HKUST-1), HKUST-1 may remain structurally stable during short-term exposure (≤ 24 h). However, prolonged exposure also resulted in irreversible alterations [34].

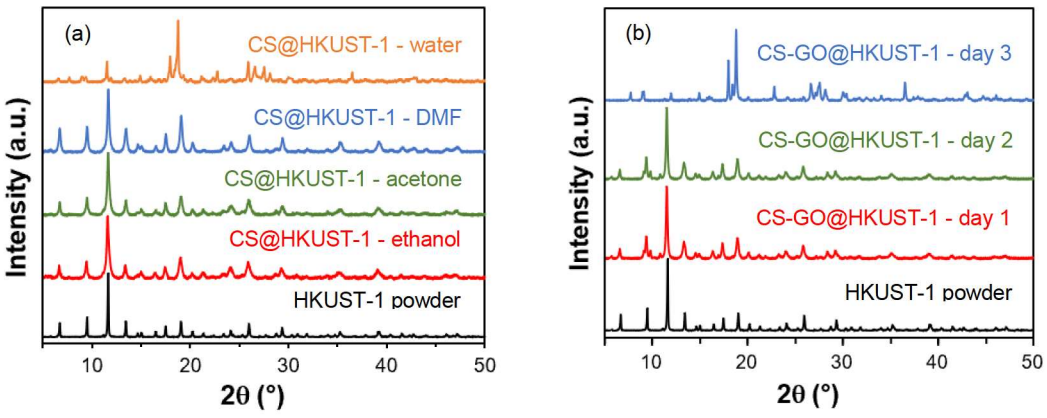

Figure 6. Powder XRD patterns of (a) CS@HKUST-1[1:2] soaked for two months at room temperature in chosen organic solvents and for one day in water, and (b) CS-GO@HKUST-1[1:2] soaked in water up to 3 days at room temperature.

In this context, the chemical stability of the CS@HKUST-1[1:2] composite was evaluated after soaking in different solvents at room temperature (see photograph, Figure S15). A prolonged contact with organic solvents (acetone, ethanol, N,N-dimethylformamide) for two months does not alter its structure (Figure 6a) nor its texture (Figure S16). However, in the presence of water, the PXRD pattern drastically change after one day, leading to the appearance of new Bragg peaks with some persisting peaks of low intensity attributed to HKUST-1 (Figure 6a). This suggests a structural transformation into a novel unidentified crystalline phase, which could not be assigned to a known compound from literature by analyzing trimesic acid-water-copper systems in the Cambridge Structural Database (CSD) (using conquest version 2023.3.0). This structural change appeared along with a significant loss of its porosity, > 94 % (Figure S16).

To understand this drastic structural modification, a comparison of PXRD patterns and IR spectra of CS@HKUST-1 with those of HKUST-1 powder soaked in water in the same conditions was performed. Figure S17 highlights that the PXRD pattern of HKUST-1 powder after soaking in water for one day differs from that of the composite. This could be attributed to the formation of different degradation products for the two materials, or that the MOF crystals embedded in the chitosan matrix may not have reached the same stage of structural transformation. The remaining surface area of the composite (approximately 55 $m^2.g^{-1}$) and visible Bragg peaks of HKUST-1 support the latter hypothesis and this suggests that the MOF has not undergone a complete degradation. In contrast, the pristine HKUST-1 powder has nearly lost its entire porosity (0.6 $m^2.g^{-1}$) together with a new set of PXRD signature (main Bragg peaks located at 2θ = 7.7; 8.9; 11.9; 21; 22.7 and 25.9 °) which has been previously reported and attributed to a mixture of $Cu(BTC)\cdot 3H_2O$ with a micropillar structure phase and a 1D coordination polymer $[CuBTC(H_2O)_3]_n$ [55]. The latter possesses a crystal structure consisting on a chain-like structure built up from the infinite connection of copper centers (square pyramidal geometry – $CuO_2(H_2O)_3$) through two carboxylate arms of the trimesate ligands [56].

The emergence of similar vibrations bands, at 1224 and 1705 cm^{-1}, are however observed in the FTIR spectra of CS@HKUST-1[1:2] composite and the HKUST-1 powder after soaking in water (Figure S18), which are attributed to C=O and C–OH bonds of carboxylic acids [52,57]. The shift of symmetric and asymmetric stretches of carboxylate from 1373, 1449 and 1615, to

1360, 1437 and 1609 cm^{-1}, respectively, suggests a weakening of the corresponding bond (C-O) following the substitution of the Cu-COO- interactions with stronger hydrogen bonds involving water, ultimately reflected by the collapse of the HKUST-1 structure [34,57]. Moreover, the shift of -OH band from 3300 cm^{-1} towards 3080 ± 30 cm^{-1} in both cases serves as strong evidence for the protonation of carboxylate groups into carboxylic acids. Thus, FTIR suggests that a major part of the materials undergoes structural transformation following hydrolysis of copper-carboxylate bonding.

On the other hand, no structural change of HKUST-1 is observed for up to 2 days in water (Figure 6.b) when GO is present within the composite beads. The same observation can be drawn from FTIR spectra (Figure S19), revealing that all the characteristic vibration bands remain similar in this condition. This is consistent with previous results where XRD patterns of HKUST-1@{graphite oxide}-n (n = 2 to 10 wt.%) remained unchanged after being in the presence of water for up to 10 h at room temperature [34]. The improved water resistance was ascribed to the coordination between the oxygen groups in graphite oxide and cationic Cu^{2+} species in HKUST-1, which efficiently prevents the coordination bonds from being attacked by water molecules.

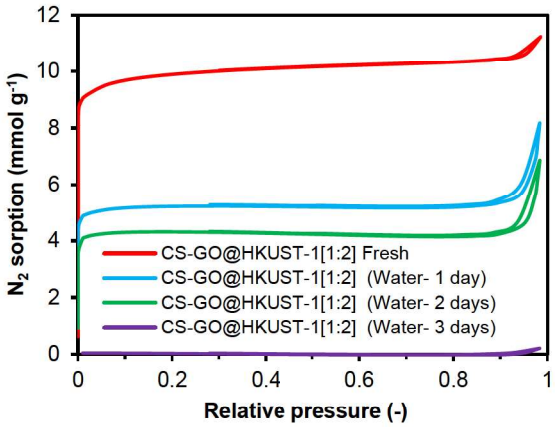

Figure 7. N_2 physisorption isotherms of CS-GO@HKUST-1[1:2] as-prepared and after soaking in water for up to three days at room temperature.

Contrarily to CS@HKUST-1[1:2] and HKUST-1 that lost respectively 94 % and 99 % of their initial S_{BET} after 1 day of water soaking, CS-GO@HKUST-1 retained 54 % (474 $m^2.g^{-1}$) and 45 % (397 $m^2.g^{-1}$) of its initial S_{BET} after water soaking for 1 and 2 days (Figure 7), respectively. However, after 3 days, the characteristic Bragg peaks of HKUST-1 fully disappear (Figure 6b), and new peaks arise (at 2θ = 7.7, 12 ,18 and 18.8°), similar to those observed for CS@HKUST-1[1:2] after one day in water (Figure 6.a). In line with this, the S_{BET} decreased sharply down to

4 $m^2.g^{-1}$ for CS-GO@HKUST-1. However, IR spectra remain almost unchanged (Figure S19) displaying all the characteristic vibrations found for the fresh composite, with only a slight change in their intensities [34].

Aside from preparing and shaping a material with enhanced textural and structural properties, as well as improved thermal and chemical stability, it is also essential to ensure that the material possesses adequate mechanical strength which is obviously a critical factor that affects its real application. Therefore, five beads of CS@HKUST-1 and CS-GO@HKUST-1 xerogels were subjected to compression tests, recording the value of 0.58 and 0.65 N until fracture, respectively (Figure S20). While these values remain low in comparison to industrial catalysts (> 20 N), it is worth noting that GO incorporation is not detrimental to the mechanical resistance of the xerogels, but rather improves it slightly.

These results altogether show that the content of incorporated GO has a neglectable impact on the structural and textural properties of HKUST-1 prepared by the *in-situ* growth strategy, while it improves clearly its stability towards hydrolysis and slightly enhances the mechanical strength of the composites. This is particularly noteworthy considering the holistic properties that can be achieved with the introduction of graphene oxide.

CO_2 adsorption. CO_2 isotherms have been first measured at 298 K for CS@HKUST-1[n(NH_2):n(Cu)] xerogels (composites prepared at 40 °C) and are presented in Figure 8.a. There is a clear dependency between the maximum CO_2 uptake and the S_{BET} of the MOF-based materials, with a maximal CO_2 uptake of 6.8 $mmol.g^{-1}$ for the pristine HKUST-1, which is in good agreement with the literature [41]. This value decreases with lower contents of HKUST-1 in the xerogels, from 3.07 $mmol.g^{-1}$ for CS@HKUST-1[1:3] and 2.60 $mmol.g^{-1}$ for CS@HKUST-1[1:2]. At even lower MOF contents, neglectable CO_2 uptake is observed (< 0.1 $mmol.g^{-1}$). Notably, the CO_2 sorption capacity of the composites with high HKUST-1 contents is significantly higher than most previously reported using similar composites, except for CS@CPO-27-CO recently reported (up to 3.10 $mmol.g^{-1}$ at 298 K) (Table S5) [58]. The CO_2 adsorption capacity of the ternary CS-GO@HKUST-1[1:2] is in line with its binary counterpart (2.55 $mmol.g^{-1}$. Figure S21b). Still, when taking into account the calculated MOF loadings, an extra decrease of CO_2 uptake of about 38.5-39.5% is observed as compared to the pristine HKUST-1 powder, related to partial pore blocking induced by the chitosan. Additional CO_2 isotherms (Figure S21a) measured with CS and CS@CuO[1:2] xerogels at 298 K show very low amounts of CO_2 adsorbed (about 0.06 $mmol.g^{-1}$). These results confirms that CO_2 adsorption is predominantly dependent on the presence of the crystalline and microporous MOF as well as its content, while CS and GO barely contribute to it.

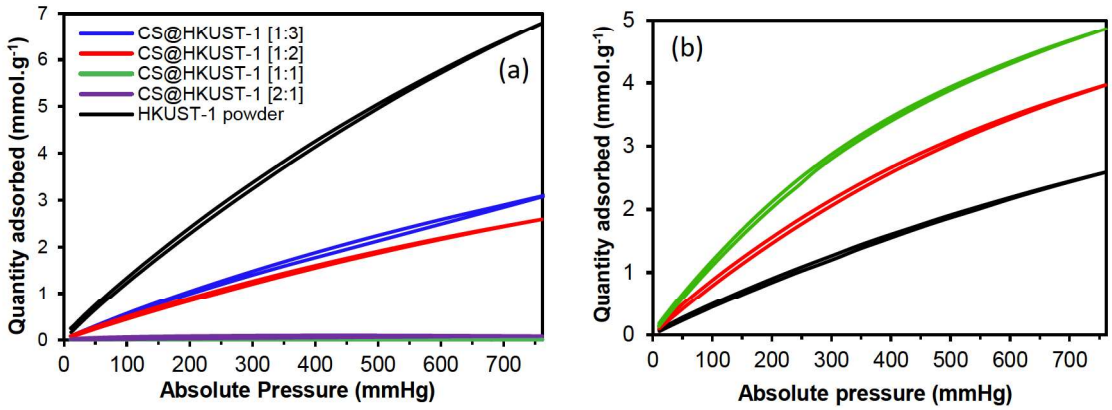

Figure 8. CO_2 adsorption isotherms (a) of HKUST-1 and the CS@HKUST-1 xerogels at 298 K and (b) of CS@HKUST-1[1:2] at 273 K (green), 283 K (red) and 298 K (black).

To get further insight on the type of interaction governing such uptake, CO_2 isotherms of the composite CS@HKUST-1[1:2] have been measured at different temperatures (Figure 8.b). As expected, the CO_2 adsorption capacity increases significantly as the temperature decreases (3.97 and 4.86 mmol.g^{-1} recorded at 283 K and 273 K, respectively). Higher recorded CO_2 uptakes following an increase of pressure and/or a decrease in temperature suggests that the adsorption process between the adsorbate (CO_2) and the adsorbent (CS@HKUST-1) is controlled by physical interactions [59]. Based on these isotherms, isosteric heats of adsorption were calculated using Clausius-Clapeyron equation [59]. The average calculated isosteric heat (Q_{st}) of adsorption is about 27 kJ.mol^{-1} (Figures S22-S23), comparable to the value obtained for HKUST-1 powder and for other HKUST-1-based composites [29,53]. Moreover, obtained Q_{st} values (24-28 kJ.mol^{-1}) are within the range of isosteric heat values typically reported for capturing single-component CO_2 streams under swing adsorption processes at industrial scale [60]. Furthermore, such a low value of Q_{st} (< 40 kJ.mol^{-1}) suggests that CO_2 sorption within CS@HKUST-1 is governed by weak physical interactions. This finding also implies that the composite material can be efficiently reused through a simple regeneration process [18].

This supposed regeneration ability of CS@HKUST-1[1:2] was experimentally tested through 10 adsorption cycles at 298 K, with a simple reactivation at 100 °C under vacuum for one night between two adsorption isotherms. As shown in Figure 9, the quantity of CO_2 adsorbed remains practically constant even after 10 cycles (2.68 mmol.g^{-1} on average), without any observable damage or alteration in beads morphology. For comparison, CS@ZIF-8 and CS@ZIF-67 composites have also shown good cycling stability, maintaining approximately 92% and 97%

of the initial CO_2 adsorption capacity after 10 and 6 cycles, albeit at lower CO_2 sorption capacities [61].

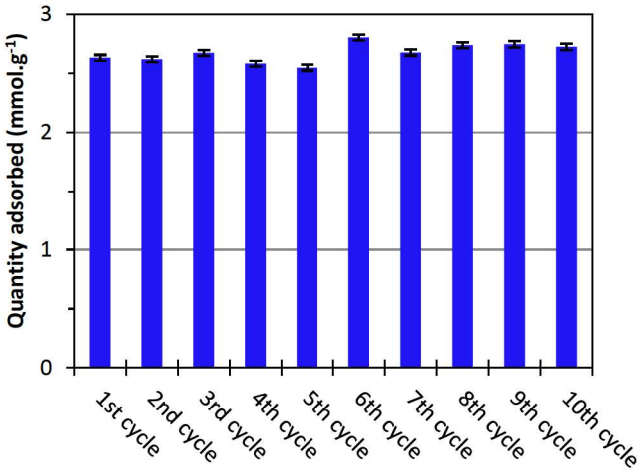

Figure 9. CO_2 adsorption uptakes of CS@HKUST-1[1:2] at 298 K and 1 bar over 10 cycles.

The textural and structural properties of the CS@HKUST-1[1:2] composite before and after CO_2 sorption cycles were compared following an eleventh cycle of CO_2 adsorption at 1 bar (no desorption). Great similarities between the powder XRD diffractograms (Figure S24.a) are observed as well as the conservation of the bands positions and the absence of ammonium carbamate bands in FTIR spectra (Figure S24.b) [65-66]. These characterizations indicate the preservation of the structural properties of CS@HKUST-1[1:2]. The slight increase in specific surface area (S_{BET}) following the adsorption-desorption cycles (Figure S24.c) could be due to a minor destruction of the polysaccharide skeletal caused by repeated activation at 100 °C. This would result in fewer pores unblocking.

Conclusions

In summary, highly porous CS@HKUST-1 based xerogel beads were developed using the *in-situ* growth strategy under mild conditions. In addition to $n(NH_2)$:n(Cu) molar ratio variation, synthesis temperature was found to play a critical role on the specific surface area and the crystalline purity of the resulting composites. Low temperature was found to be adapted for the preparation of pure HKUST-1 phase within CS matrix, resulting in high surface area. As HKUST-1 is highly sensitive to the presence of water, graphene oxide was incorporated at the optimal conditions to prepare highly porous CS-GO@HKUST-1 composites (up to 878 $m^2.g^{-1}$) with greatly improved water stability compared to pristine HKUST-1 and CS@HKUST-1. N_2 adsorption proved that 45 % of the initial textural properties were retained after soaking CS-

GO@HKUST-1 in water up to two days, while microporous structure entirely collapsed (-94 % of S_{BET}) for CS@HKUST-1 after only one day. Aside from enhancing chemical stability, GO is also found to have a slight positive impact on mechanical beads resistance. The performance of the prepared composites for CO_2 sorption was also studied, and an average CO_2 uptake of 2.68 $mmol.g^{-1}$ could be reached at 298 K and 1 bar with CS@HKUST-1 beads while preserving the same performances for more than 10 cycles of adsorption-desorption.

Acknowledgments

The Chevreul Institute is thanked for its help in the development of this work through the ARCHI-CM project supported by the "Ministere de l'Enseignement Superieur de la Recherche et de l'Innovation", the region "Hauts-de-France", the ERDF program of the European Union and the "Metropole Europeenne de Lille. Y. Khadiri is grateful to the University of Lille and the University Euromed Fez for the PhD grant. The authors would like to thank Martine Trentesaux for her help with Raman spectroscopy analysis, Laurence Burylo for the powder X-ray diffraction and diffusion facility and Alexandre Fadel for his help withy SEM analyses.

Associated content

Detailed synthesis protocols, additional characterization of samples by SEM, EDS, XRD, FTIR, TGA, and N_2-physisorption isotherms; tables with additional experimental and bibliographic data; additional CO_2 physisorption isotherms and thermodynamic calculations.

References

[1] C.-C. Chang, "A multivariate causality test of carbon dioxide emissions, energy consumption and economic growth in China," *Appl. Energy*, 87 (2010) 3533–3537, doi: 10.1016/j.apenergy.2010.05.004.

[2] S. M. R. Razavi, M. Rezakazemi, A. B. Albadarin, and S. Shirazian, "Simulation of CO_2 absorption by solution of ammonium ionic liquid in hollow-fiber contactors," *Chem. Eng. Process. Process Intensif.*, 108 (2016) 27–34, doi: 10.1016/j.cep.2016.07.001.

[3] N. Hajilary, A. Shahi, and M. Rezakazemi, "Evaluation of socio-economic factors on CO2 emissions in Iran: Factorial design and multivariable methods," *J. Clean. Prod.*, 189 (2018) 108–115, doi: 10.1016/j.jclepro.2018.04.067.

[4] M. Khraisheh, S. Mukherjee, A. Kumar, F. Al Momani, G. Walker, and M. J. Zaworotko, "An overview on trace CO_2 removal by advanced physisorbent materials," *J. Environ. Manage.*, 255 (2020) 109874, doi: 10.1016/j.jenvman.2019.109874.

[5] S. Krachuamram, K. C. Chanapattharapol, and N. Kamonsutthipaijit, "Synthesis and characterization of NaX-type zeolites prepared by different silica and alumina sources and their CO_2 adsorption properties," *Microporous Mesoporous Mater.*, 310 (2021) 110632, doi: 10.1016/j.micromeso.2020.110632.

[6] K. Malini, D. Selvakumar, and N. S. Kumar, "Activated carbon from biomass: Preparation, factors improving basicity and surface properties for enhanced CO_2 capture capacity – A review," *J. CO_2 Util.*, 67 (2023) 102318, doi: 10.1016/j.jcou.2022.102318.

[7] N. H. M. Hossein Tehrani, M. Ardjmand, M. Bazmi, A. Rashidi, and H. R. M. Zadeh, "Polydopamine-modified mesoporous silica materials as a novel adsorbent for superior CO2 adsorption: Experimental and DFT study," *J. Environ. Chem. Eng.*, 11 (2023) 110451, doi: 10.1016/j.jece.2023.110451.

[8] K. Sumida, D. L. Rogow, J. A. Mason, T. M. McDonald, E. D. Bloch, Z. R. Herm, T. H. Bae, and J. R. Long, "Carbon Dioxide Capture in Metal–Organic Frameworks," *Chem. Rev.*, 112 (2012) 724–781, doi: 10.1021/cr2003272.

[9] A. Rosado, A. Borrás, J. Fraile, J. A. R. Navarro, F.Suárez-García, K. C. Stylianou, A. M. López-Periago, J. G. Planas, C. Domingo, A.Yazdi., "HKUST-1 Metal–Organic Framework Nanoparticle/Graphene Oxide Nanocomposite Aerogels for CO_2 and CH_4 Adsorption and Separation," *ACS Appl. Nano Mater.*, 4 (2021) 12712–12725, doi: 10.1021/acsanm.1c03301.

[10] J. Lin, Tai T. T. Nguyen, R.Vaidhyanathan, J. Burner, J. M. Taylor, H. Durekova, F. Akhtar, R. K. Mah, O. Ghaffari-Nik, S. Marx, N. Fylstra, S. S. Iremonger, K. W. Dawson, P. Sarkar, P. Hovington, A. Rajendran, T. K. Woo, G. K. H. Shimizu, "A scalable metal-organic framework as a durable physisorbent for carbon dioxide capture," *Science*, 374 (2021) 1464–1469, doi: 10.1126/science.abi7281.

[11] U. Ko¨kçam-Demir, A. Goldman, L. Esrafili, M. Gharib, A. Morsali, O. Weingart , C. Janiak, "Coordinatively unsaturated metal sites (open metal sites) in metal–organic frameworks: design and applications," *Chem. Soc. Rev.*, 49 (2020) 2751–2798, doi: 10.1039/C9CS00609E.

[12] H. Furukawa, N. Ko, Y. Go, N. Aratani, S. B. Choi,?E. Choi, A. Ö. Yazaydin, R. Q. Snurr, M. O'Keeffe, J. Kim, O. M. Yaghi, "Ultrahigh Porosity in Metal-Organic Frameworks," *Science*, 329 (2010) 424–428, doi: 10.1126/science.1192160.

[13] S. Gulati, S. Vijayan, Mansi, S. Kumar, B. Harikumar, M. Trivedi, R. S. Varma, "Recent advances in the application of metal-organic frameworks (MOFs)-based nanocatalysts for direct conversion of carbon dioxide (CO_2) to value-added chemicals," *Coord. Chem. Rev.*, 474 (2023) 214853, doi: 10.1016/j.ccr.2022.214853.

[14] S. S.-Y. Chui, S. M.-F. Lo, J. P. H. Charmant, A. G. Orpen, and I. D. Williams, "A Chemically Functionalizable Nanoporous Material [Cu_3 $(TMA)_2$ $(H_2O)_3]_n$," *Science*, 283 (1999) 1148–1150, doi: 10.1126/science.283.5405.1148.
[15] X. Mu, Y. Chen, E. Lester, and T. Wu, "Optimized synthesis of nano-scale high quality HKUST-1 under mild conditions and its application in CO_2 capture," *Microporous Mesoporous Mater.*, 270 (2018) 249–257, doi: 10.1016/j.micromeso.2018.05.027.
[16] Y.-K. Seo, G. Hundal, I. T. Jang, Y. K. Hwang, C.-H. Jun, and J.-S. Chang, "Microwave synthesis of hybrid inorganic–organic materials including porous Cu3(BTC)2 from Cu(II)-trimesate mixture," *Microporous Mesoporous Mater.*, 119 (2009) 331–337, doi: 10.1016/j.micromeso.2008.10.035.
[17] Y. Hijikata and S. Sakaki, "Interaction of Various Gas Molecules with Paddle-Wheel-Type Open Metal Sites of Porous Coordination Polymers: Theoretical Investigation," *Inorg. Chem.*, 53 (2014) 2417–2426, doi: 10.1021/ic402172v.
[18] S. Samipour, M. D. Manshadi, and P. Setoodeh, "CO_2 removal from biogas and syngas," in *Advances in Carbon Capture*, Elsevier, (2020). 455–477, doi: 10.1016/B978-0-12-819657-1.00020-7.
[19] H. Zhao, N. Zhao, Q. Wang, F. Li, F. Wang, S. Fan, E.V. Matus, Z. R. Ismagilov, L. Li, F. Xiao, "Adsorption equilibrium and kinetics of CO_2 on mesocellular foams modified HKUST-1: Experiment and simulation," *J. CO_2 Util.*, 44 (2021) 101415, doi: 10.1016/j.jcou.2020.101415.
[20] B. Yeskendir, J.-P. Dacquin, Y. Lorgouilloux, C. Courtois, S. Royer, and J. Dhainaut, "From metal–organic framework powders to shaped solids: recent developments and challenges," *Mater. Adv.*, 2 (2021) 7139–7186, 2021, doi: 10.1039/D1MA00630D.
[21] T. Tian, Z. Zeng, D. Vulpe, M. E. Casco, G. Divitini, P. A. Midgley, J. Silvestre-Albero, J. Tan, P. Z. Moghadam, D. Fairen-Jimenez, "A sol–gel monolithic metal–organic framework with enhanced methane uptake," *Nat. Mater.* vol. 17 (2018) 174–179, doi: 10.1038/nmat5050.
[22] H. Zhu, Q. Zhang, and S. Zhu, "Alginate Hydrogel: A Shapeable and Versatile Platform for *in Situ* Preparation of Metal–Organic Framework–Polymer Composites," *ACS Appl. Mater. Interfaces*, 8 (2016) 17395–17401, doi: 10.1021/acsami.6b04505.
[23] H. Musarurwa and N. T. Tavengwa, "Application of polysaccharide-based metal organic framework membranes in separation science," *Carbohydr. Polym.*, 275 (2022) 118743, doi: 10.1016/j.carbpol.2021.118743.
[24] S. El Hankari, M. Bousmina, and A. El Kadib, "Biopolymer@Metal-Organic Framework Hybrid Materials: A Critical Survey," *Prog. Mater. Sci.*, 106 (2019)100579, doi: 10.1016/j.pmatsci.2019.100579.
[25] A. El Kadib, "Green and Functional Aerogels by Macromolecular and Textural Engineering of Chitosan Microspheres," *Chem. Rec.*, 20 (2020) 753–772, doi: 10.1002/tcr.201900089.
[26] S. Takeshita, S. Zhao, W. J. Malfait, and M. M. Koebel, "Chemistry of Chitosan Aerogels: Three-Dimensional Pore Control for Tailored Applications," *Angew. Chem. Int. Ed.*, 60 (2021) 9828–9851, doi: 10.1002/anie.202003053.
[27] A. Balakrishnan, M. M. Jacob, N. Dayanandan, M. Chinthala, M. Ponnuchamy, D. N. Vo, S. Appunnid, A. S. Gajendhrane., "Chitosan/metal organic frameworks for environmental, energy, and bio-medical applications: a review," *Mater. Adv.*, 4 (2023) 5920–5947, doi: 10.1039/D3MA00413A.
[28] R. Zhao, T. Ma, S. Zhao, II. Rong, Y. Tian, and G. Zhu, "Uniform and stable immobilization of metal-organic frameworks into chitosan matrix for enhanced tetracycline removal from water," *Chem. Eng. J.*, 382 (2020) 122893, doi: 10.1016/j.cej.2019.122893.

[29] N. Hammi, M. Bonneau, A. El Kadib, S. Kitagawa, T. Loiseau, C. Volkringer, S. Royer, J. Dhainaut., "Enhanced Gas Adsorption in HKUST-1@Chitosan Aerogels, Cryogels, and Xerogels: An Evaluation Study," *ACS Appl. Mater. Interfaces*, 15 (2023) 53395–53404, doi: 10.1021/acsami.3c10408.
[30] A. J. Howarth, Y. Liu, P. Li, Z. Li, T. C. Wang, J. T. Hupp, O. K. Farha., "Chemical, thermal and mechanical stabilities of metal–organic frameworks," *Nat. Rev. Mater.*, 1 (2016) 1-15, doi: 10.1038/natrevmats.2015.18.
[31] M. P. Singh, N. R. Dhumal, H. J. Kim, J. Kiefer, and J. A. Anderson, "Influence of Water on the Chemistry and Structure of the Metal–Organic Framework $Cu_3(btc)_2$," *J. Phys. Chem. C*, 120 (2016) 17323–17333, doi: 10.1021/acs.jpcc.6b02906.
[32] Q. Miao, L. Jiang, J. Yang, T. Hu, S. Shan, H. Su, F. Wu., "MOF/hydrogel composite-based adsorbents for water treatment: A review," *J. Water Process Eng.*, 50 (2022) 103348, doi: 10.1016/j.jwpe.2022.103348.
[33] S. J. Yang, J. Y. Choi, H. K. Chae, J. H. Cho, K. S. Nahm, and C. R. Park, "Preparation and Enhanced Hydrostability and Hydrogen Storage Capacity of CNT@MOF-5 Hybrid Composite," Chem. Mater., 21(2009) 1893–1897, doi: 10.1021/cm803502y.
[34] Y. Li, J. Miao, X. Sun, J. Xiao, Y. Li, H. Wang, Q. Xia, Z. Li, "Mechanochemical synthesis of Cu-BTC@GO with enhanced water stability and toluene adsorption capacity," Chem. Eng. J., 298 (2016) 191–197, doi: 10.1016/j.cej.2016.03.141.
[35] Z. Zhang, W. Huang, X. Li, X. Wang, Y. Zheng, B. Yan, C. Wu, "Water-stable composite of HKUST-1 with its pyrolysis products for enhanced CO2 capture capacity," Inorg. Chem. Commun., 146 (2022) 110063, doi: 10.1016/j.inoche.2022.110063.
[36] R. K. Singh, R. Kumar, and D. P. Singh, "Graphene oxide: strategies for synthesis, reduction and frontier applications," *RSC Adv.*, 6 (2016) 64993–65011, doi: 10.1039/C6RA07626B.
[37] P. Jagódka, K. Matus, and A. Łamacz, "On the HKUST-1/GO and HKUST-1/rGO Composites: The Impact of Synthesis Method on Physicochemical Properties," *Molecules*, 27 (2022) 7082, doi: 10.3390/molecules27207082.
[38] A. Kumar, A. Saxena, A. De, R. Shankar, S. Mozumdar "Facile synthesis of size-tunable copper and copper oxide nanoparticles using reverse microemulsions," *RSC Adv.*, 3 (2013) 5015-5021, doi: 10.1039/C3RA23455J.
[39] Y. Wang, A. Pitto-Barry, A. Habtemariam, I. Romero-Canelon, P. J. Sadler, and N. P. E. Barry, "Nanoparticles of chitosan conjugated to organo-ruthenium complexes," *Inorg. Chem. Front.*, 3 (2016) 1058–1064, doi: 10.1039/C6QI00115G.
[40] T. Zelenka, K. Simanova, R. Saini, G. Zelenkova, S. Nehra, A. Sharma, M. Almasi, "Carbon dioxide and hydrogen adsorption study on surface-modified HKUST-1 with diamine/triamine," *Sci. Rep.*, 12 (2022) 17366, doi: 10.1038/s41598-022-22273-2.
[41] F. Xu, Y. Yu, J. Yan, Q. Xia, H. Wang, J. Li, Z. Li., "Ultrafast room temperature synthesis of GrO@HKUST-1 composites with high CO2 adsorption capacity and CO_2/N_2 adsorption selectivity," *Chem. Eng. J.*, 303 (2016) 231–237, doi: 10.1016/j.cej.2016.05.143.
[42] S. Frindy, A. el Kadib, M. Lahcini, A. Primo, and H. García, "Copper Nanoparticles Stabilized in a Porous Chitosan Aerogel as a Heterogeneous Catalyst for C−S Cross-coupling," *ChemCatChem*, 7 (2015) 3307–3315, doi: 10.1002/cctc.201500565.
[43] P. Cazón, A. Antoniewska, J. Rutkowska, and M. Vázquez, "Evaluation of easy-removing antioxidant films of chitosan with Melaleuca alternifolia essential oil," *Int. J. Biol. Macromol.*, 186 (2021) 365–376, doi: 10.1016/j.ijbiomac.2021.07.035.
[44] W. Zhang, T. Huang, Y. Ren, Y. Wang, R. Yu, J. Wang, Q. Tu., "Preparation of chitosan crosslinked with metal-organic framework (MOF-199)@aminated graphene oxide aerogel

for the adsorption of formaldehyde gas and methyl orange," *Int. J. Biol. Macromol.*, 193 (2021) 2243–2251, doi: 10.1016/j.ijbiomac.2021.11.056.
[45] F. Di Renzo, R. Valentin, M. Boissière, A. Tourrette, G. Sparapano, K. Molvinger, J. Devoisselle, C. Gérardin, F. Quignard., "Hierarchical Macroporosity Induced by Constrained Syneresis in Core−Shell Polysaccharide Composites," *Chem. Mater.*, 17 (2005) 4693–4699, doi: 10.1021/cm0503477.
[46] F. Ambroz, T. J. Macdonald, V. Martis, I. P. Parkin, "Evaluation of the BET Theory for the Characterization of Meso and Microporous MOFs," *Small Methods*, 2 (2018) 1800173, doi: 10.1002/smtd.201800173.
[47] A. Domán, J. Madarász, G. Sáfrán, Y. Wang, K. László, "Copper benzene-1,3,5-tricarboxylate (HKUST-1) – graphene oxide pellets for methane adsorption," *Microporous Mesoporous Mater.*, 316 (2021) 110948, doi: 10.1016/j.micromeso.2021.110948.
[48] F. Zhao, B. Yu, Z. Yue, T. Wang, X. Wen, Z. Liu, C. Zhao., "Preparation of porous chitosan gel beads for copper(II) ion adsorption," *J. Hazard. Mater.*, 147 (2007) 67–73, doi: 10.1016/j.jhazmat.2006.12.045.
[49] C. Chartier, S. Buwalda, H. Van Den Berghe, B. Nottelet, T. Budtova, "Tuning the properties of porous chitosan: Aerogels and cryogels," *Int. J. Biol. Macromol.*, 202 (2022) 215–223, doi: 10.1016/j.ijbiomac.2022.01.042.
[50] K. Schlichte, T. Kratzke, S. Kaskel, "Improved synthesis, thermal stability and catalytic properties of the metal-organic framework compound $Cu_3(BTC)_2$," *Microporous Mesoporous Mater.*, 73 (2004) 81–88, doi: 10.1016/j.micromeso.2003.12.027.
[51] J. Cortés-Sú arez, V. Celis-Arias, II. Beltrán, A. Tejeda-Cruz, I. A. Ibarra, J. E. Romero-Ibarra, E. Sánchez-González, S. Loera-Serna., "Synthesis and Characterization of an SWCNT@HKUST-1 Composite: Enhancing the CO_2 Adsorption Properties of HKUST-1," *ACS Omega*, vol. 4 (2019) 5275–5282, doi: 10.1021/acsomega.9b00330.
[52] J. B. DeCoste, G. W. Peterson, B. J. Schindler, K. L. Killops, M. A. Browe, and J. J. Mahle, "The effect of water adsorption on the structure of the carboxylate containing metal–organic frameworks Cu-BTC, Mg-MOF-74, and UiO-66," *J. Mater. Chem. A*, 1, (2013) 11922, doi: 10.1039/c3ta12497e.
[53] N. Al-Janabi, P. Hill, L. Torrente-Murciano , A. Garforth, P. Gorgojo, F. Siperstein, X. Fan., "Mapping the Cu-BTC metal–organic framework (HKUST-1) stability envelope in the presence of water vapour for CO_2 adsorption from flue gases," *Chem. Eng. J.*, 281 (2015) 669–677, doi: 10.1016/j.cej.2015.07.020.
[54] R. Giovine, F. Pourpoint, S. Duval, O. Lafon, J. Amoureux, T. Loiseau, C. Volkringer, "The Surprising Stability of $Cu_3(btc)_2$ Metal–Organic Framework under Steam Flow at High Temperature," *Cryst. Growth Des.*, 18 (2018) 6681–6693, doi: 10.1021/acs.cgd.8b00931.
[55] N. T. Phuong, D. T. Hai, T. Doneux, N. H. Nam, and D. T. M. Thanh, "Synthesis of metal organic framework based on Cu and benzene-1,3,5-tricarboxylic acid (H_3BTC) by potentiodynamic method for CO2 adsorption," *Vietnam J. Chem.*, 61 (2023) 210–219, doi: 10.1002/vjch.202200125.
[56] R. Pech and J. Pickardt, "catena-Triaqua-μ-[1,3,5-benzenetricarboxylato(2–)]-copper(II)," *Acta Crystallogr. C*, 44 (1988) 992–994, doi: 10.1107/S0108270188002902.
[57] J. B. DeCoste, G. W. Peterson, H. Jasuja, T. G. Glover, Y. Huang, and K. S. Walton, "Stability and degradation mechanisms of metal–organic frameworks containing the Zr6O4(OII)4 secondary building unit," *J. Mater. Chem. A*, 1 (2013) 5642–5650, doi: 10.1039/C3TA10662D.
[58] Y. Khadiri, C. Volkringer, S. Royer, A. El Kadib, T. Loiseau, and J. Dhainaut, "Chemical shaping of CPO-27-M (M = Co, Ni) through an *in-situ* crystallization within chitosan

hydrogels," *Chem. Commun*, 2024, doi: 10.1039/D4CC02082K.
[59] M. Anas, A. G. Gönel, S. E. Bozbag, and C. Erkey, "Thermodynamics of Adsorption of Carbon Dioxide on Various Aerogels," *J. CO_2 Util.*, 21 (2017) 82–88, doi: 10.1016/j.jcou.2017.06.008.
[60] J. M. Simmons, H. Wu, W. Zhou, and T. Yildirim, "Carbon capture in metal–organic frameworks—a comparative study," *Energy Environ. Sci.*, 4 (2011) 2177–2185, doi: 10.1039/C0EE00700E.
[61] N. Hammi, N. Couzona, T. Loiseau, C. Volkringer, A. El Kadib, S. Royer, J. Dhainauta, "Hierarchically porous ZIF-67/chitosan beads with high surface area and strengthened mechanical properties: Application to CO_2 storage," *Mater. Today Sustain.*, 22 (2023) 100394, doi: 10.1016/j.mtsust.2023.100394.
[62] J. A. O. Chagas, G. O. Crispim, B. P. Pinto, R. A. S. San Gil, and C. J. A. Mota, "Synthesis, Characterization, and CO $_2$ Uptake of Adsorbents Prepared by Hydrothermal Carbonization of Chitosan," *ACS Omega*, 5 (2020) 29520–29529, doi: 10.1021/acsomega.0c04470.
[63] N. Hedin and Z. Bacsik, "Perspectives on the adsorption of CO2 on amine-modified silica studied by infrared spectroscopy," *Curr. Opin. Green Sustain. Chem.*, 16 (2019) 13–19, doi: 10.1016/j.cogsc.2018.11.010.

Graphical abstract